Mon. Not. R. astr. Soc. (1981) **196**, 857–887

Detailed observations of NGC 4151 with *IUE* – I Low dispersion data up to 1979 January★

M. V. Penston[1]†, A. Boksenberg[2], G. E. Bromage[3], J. Clavel[1]‡, A. Elvius[4], P. M. Gondhalekar[5], C. Jordan[6], J. Lind[7], L. Lindegren[7], G. C. Perola[8], M. Pettini[2]†, M. A. J. Snijders[2], E. G. Tanzi[9], M. Tarenghi[10] and M. H. Ulrich[10]

[1]*Astronomy Division, ESTEC, ESA Villafranca Satellite Tracking Station, Apartado 54065, Madrid, Spain*

[2]*Department of Physics and Astronomy, University College London, Gower Street, London WC1E 6BT*

[3]*Astrophysics Group, Rutherford and Appleton Laboratories, Chilton, Didcot, Oxfordshire OX11 0QX*

[4]*Stockholm Observatory, Saltsjobaden, Sweden*

[5]*Rutherford and Appleton Laboratories, Chilton, Didcot, Oxfordshire OX11 0QX*

[6]*Department of Theoretical Physics, University of Oxford, Oxford*

[7]*Lund Observatory, Lund, Sweden*

[8]*Istituto di Fisica dell'Universitá, Milan, Italy*

[9]*Istituto di Fisica Cosmica, CNR, Milan, Italy*

[10]*European Southern Observatory, Garching bei München, Germany*

Received 1981 January 9; in original form 1980 October 6

Summary. This paper reports low resolution ultraviolet spectroscopic monitoring of NGC 4151 with *IUE* in the period 1978 February to 1979 January. Observations were made at seven different epochs.

Continuum points can be isolated in both longwave (1950–3250 Å) and, with some difficulty, shortwave (1150–1950 Å) regions. The observed continuum shows a long wavelength $f_\nu \propto \nu^{-2}$ component and a flatter short wavelength component. There is some evidence that these do not vary exactly together. A value for $E(B-V)$ between 0.05 and 0.10 mag is derived from the weakness of the interstellar λ 2200 Å feature.

★Based on observations with the *International Ultraviolet Explorer* collected at the European Space Agency's Villafranca Satellite Tracking Station.

† Present address: Royal Greenwich Observatory, Herstmonceux Castle, Hailsham, East Sussex BN27 1RP.

‡ Present address: Observatoire de Meudon, Meudon, France.

Fifteen absorption features are identified and their equivalent widths measured. Some arise from metastable levels, some are variable and others are stronger than can be accounted for by the interstellar media of our Galaxy and of the NGC 4151 galaxy alone. Most arise in the nucleus of NGC 4151. Velocity variations in the absorption region are indicated by changing V/R ratios in the overall C IV feature.

The Si IV lines are unsaturated and must therefore be broad ($b \gtrsim 800$ to 1300 km s^{-1}). The lower limit to the absorbing column n (H) $> 3 \times 10^{19}$ cm^{-2} is much less than the X-ray column (10^{23} cm^{-2}) but this latter amount could be present but escape detection if in the form of clouds with low velocity dispersions.

The strong emission lines include those seen in quasars; weaker features including some unidentified ones are also discussed. The intensities of the high-ionization emission lines are variable, as are the linewidths of C IV.

Most variable parameters, except the C IV V/R ratio and possibly the short wavelength continuum excess, vary in phase or anti-phase with the continuum and may be explained in terms of changing ionization conditions in the absorption and emission regions.

1 Introduction

NGC 4151 is the brightest Type 1 Seyfert galaxy and has attracted much observational attention at all wavebands. Optical spectroscopy (e.g. Boksenberg *et al.* 1975) shows the broad permitted lines (FWZI ~ 8000 km s^{-1}) which are the defining characteristic of this type of Seyfert, but in NGC 4151 the narrow forbidden lines and cores to the permitted lines (FWZI ~ 1200 km s^{-1}) are quite strong, earning the galaxy the refined classification Seyfert class 1.5 (Osterbrock 1977). Variable absorption in the optical is also known in the Balmer lines and in He I λ3889 (Anderson & Kraft 1969; Cromwell & Weymann 1970; Anderson 1974). There are also variations in the optical and infrared continua (e.g. Rieke 1978; Penston *et al.* 1974). NGC 4151 is a radio (e.g. Kellerman & Pauliny-Toth 1968) and an X-ray (e.g. Gursky *et al.* 1971) source. The X-ray data show variations both in intensity and in the column of absorbing material along the line of sight (Barr *et al.* 1977).

NGC 4151 has been observed in the ultraviolet by Davidsen & Hartig (1978), Boksenberg *et al.* (1978) and Penston *et al.* (1979). A preliminary version of some of the present results was given by Baldwin *et al.* (1979) and Boksenberg *et al.* (1980) as conference reports. The purpose of this paper is to give a further discussion of data on this galaxy taken over the first year of the guest observer programme of the *International Ultraviolet Explorer* (*IUE*) by a widespread European collaboration. It covers a data description (Section 2), the continuum (Section 3), the absorption lines (Section 4), the emission lines (Section 5), and a discussion of the variability (Section 6). We anticipate a further paper to discuss later observations and other refined analyses of the presently reported results.

2 Data description

2.1 ACQUISITION OF DATA

The *International Ultraviolet Explorer* (*IUE*) is an ultraviolet spectroscopy satellite and has been described by Boggess *et al.* (1978a, b). All the observations discussed here were made at low dispersion and a full list of the observing details is given in Table 1. We include in this table the commissioning observations reported earlier by Boksenberg *et al.* (1978).

Table 1. Journal of observations.

Date	Image number	Aperture	Exposure time (min)	m_{FES}
1978				
Feb. 11.82	SWR 1025	L	60	
Feb. 12.	LWP 1028	L	120	
Feb. 28.70	SWR 1064	L	120	
May 08.29	SWP 1505	S	40	
May 09.28	LWR 1463	S	60	
May 11.05	SWP 1518	S	240	11.95 ± 0.11
May 11.28	SWP 1519	S	60	
May 12.05	SWP 1523	S	120	
May 12.14	LWR 1476	S	120	
May 12.23	SWP 1524	S	120	
July 24.85	LWR 1885	L	30	
July 24.89	SWP 2098	S	60	12.11 ± 0.09
July 24.93	SWP 2098	L	30	12.00 ± 0.08
Aug. 02.09	SWP 2171	L	30	
Oct. 19.68	SWP 3048	S	60	
Oct. 19.73	SWP 3048	L	30	
Oct. 19.75	LWR2650	L	25	12.04 ± 0.06
Oct. 19.77	SWP 3049	L	25	
Oct. 19.80	LWR2651	L	25	
Dec. 09.47	LWR 3129	L	30	
Dec. 09.49	SWP 3557	L	30	12.16 ± 0.08
Dec. 09.52	SWP 3557	S	60	
Dec. 09.56	LWR 3130	L	60	
Dec. 25.46	–	–	–	12.22 ± 0.15
1979				
Jan. 21.53	LWR 3538	L	25	
Jan. 21.55	SWP 3971	L	25	
Jan. 21.57	SWP 3971	S	60	12.17 ± 0.08
Jan. 21.62	LWR 3539	L	25	
Jan. 21.64	SWP 3972	L	25	

The normal observing procedure called for two large-aperture exposures in each of the short- and longwave cameras at each epoch to provide verification of any variations; generally, in the shortwave region, one observation was also made in the small aperture in order to have a good measure of the Lyman α emission intensity at each epoch. Optimum exposure times when the object is bright were found to be 25–30 min and 50–60 min in large and small apertures respectively. A large-aperture exposure of 40–50 min was added when the object was faint or when a better signal-to-noise ratio in the continuum was required. However, in the earliest observations of 1978 February and May this procedure was still being developed and, for example, in 1978 May only small-aperture observations were made. Resulting difficulties in reduction are discussed in Sections 2.2 and 2.3.

The data were initially reduced using the standard IUESIPS package. For the data after 1978 June, however, this package contained a serious error in the intensity transfer function (ITF) for the shortwave prime (SWP) camera. This error was corrected in two ways: (i) by applying a variant of the method of Cassatella & Ponz (1979) as implemented at the European Southern Observatory; and (ii) by a correction of the geometrically and photometrically corrected image and subsequent re-extraction (Snijders 1980). These methods

were compared and found to be in generally good agreement. As detailed in Section 2.2, the second method was adopted to give a uniform data reduction procedure for scientific analysis.

Table 1 also contains an optical magnitude for the galaxy as measured with *IUE*'s fine error sensor (FES) on many of the dates of observation including the high dispersion observation on 1978 December 25 by Penston *et al.* (1979). The calibration of these FES magnitudes for stars is discussed by Stickland (1980). Note that, for stars with no emission lines

$$m_{\mathrm{FES}} = V + 0.28\,(B-V).$$

For bright stars the standard error can attain 0.05 mag but errors given here are deduced from the internal scatter of observations taken the same day. It should be emphasized, however, that since NGC 4151 is an extended source and because the FES aperture is large (12 arcsec square) and offset from the nucleus (by 4 arcsec), contamination by starlight from the surrounding galaxy must be important. Any variations of the nucleus will be diluted in m_{FES} by this effect. The data of Penston *et al.* (1974) show that about half the light in the FES aperture will be from stars when the nucleus is at near-'normal' brightness.

2.2 DATA REDUCTION

A uniform system of image processing and data reduction has been applied to all *IUE* spectra presented here (and to the later low resolution data on NGC 4151 which will be presented in a second paper), with the exception of the earliest epochs of 1978 February and May.

For the SWP data the spectra were re-extracted from the geometrically and photometrically corrected image (file 2) after applying a correction for the ITF error where necessary (Snijders 1980). The LWR spectra used the IUE standard image processing system (IUESIPS) except for an improved background correction. After blemishes (fiducials, particle events) were removed from the *IUE*-supplied (file 5) background (Snijders 1980) it was smoothed as in IUESIPS and a new net spectrum derived.

Small-aperture spectra were scaled to absolute flux units by calculating transmission factors from the ratio of 50 Å-bin fluxes through the small and large apertures on the same day. The transmission varied between 20 and 55 per cent.

During the international commissioning phase, spectra were obtained on 1978 February 11 and 28. The data of February 11 are of poor quality and not used here, but the February 28 SWR spectrum is of excellent quality (Boksenberg *et al.* 1978) and is included. The relative calibration of this spectrum is known (Boksenberg *et al.* 1978; Snijders 1979) but there is an unknown scale factor in the absolute calibration due to variable large-aperture transmission during the commissioning phase.

The 1978 May data pose two problems: only small aperture data are available and for these early data the SWP extraction method used for all later spectra cannot always be applied (Snijders 1980). The SWP May spectra were treated in the same way as the LWR data: the IUESIPS extraction was used with a background cleaned of defects. They were then put on a preliminary absolute flux scale by assuming first that the 1978 July absolute flux scale is also valid for May and then calculating a mean May spectrum. An approximate absolute calibration for the 1978 February and May observations was then made assuming that the C III] + Si III] λ1900 emission feature had the same strength as at other epochs when the N V and Si IV absorption lines had comparable strength (1978 October, 1979 end May and June). As will be described later, the C III] + Si III] feature only varies slightly in strength, possibly in phase with the ultraviolet continuum and the high-ionization absorption lines.

The position of the object in the large aperture is not exactly known so that there may be wavelength shifts between spectra. The zero points for each spectrum were chosen to bring

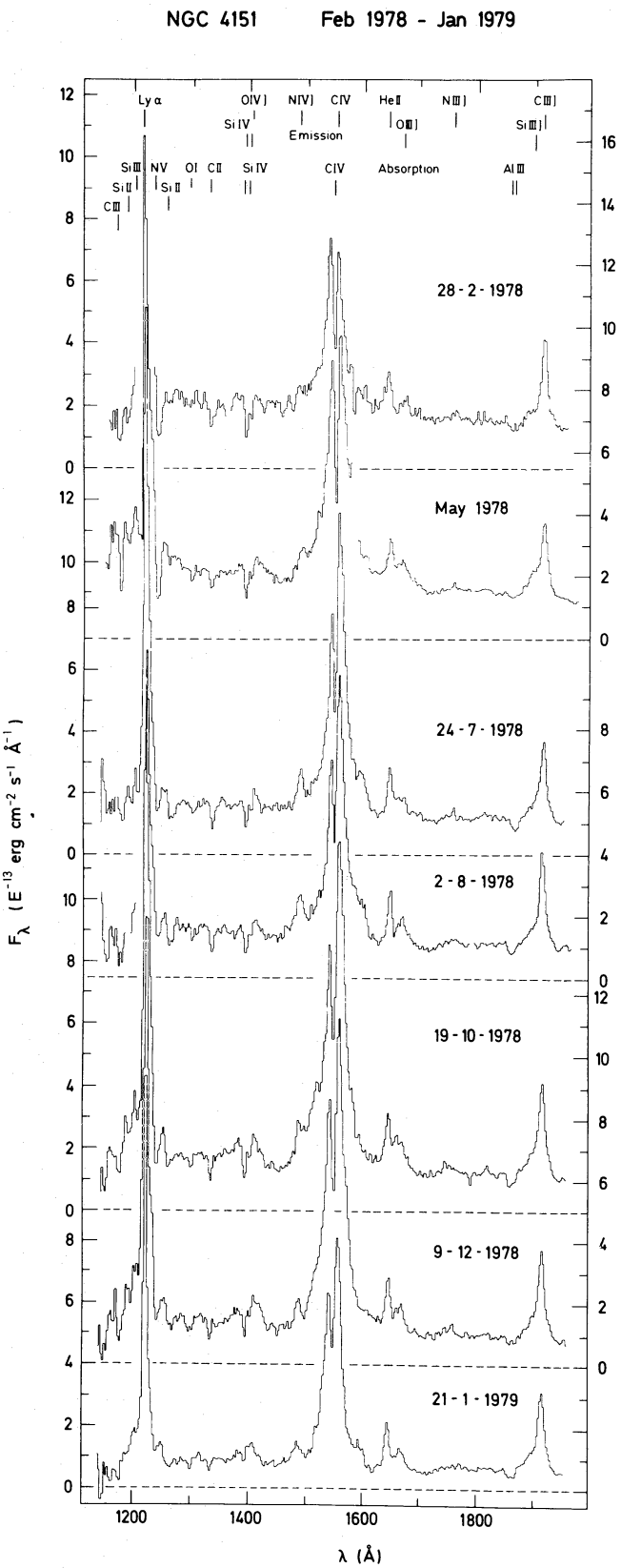

Figure 1. Montage of the short wavelength *IUE* spectra of NGC 4151 taken in the first year of the satellite. Note the variations in continuum level, emission intensity and linewidth, and absorption equivalent widths and velocity with respect to the emission.

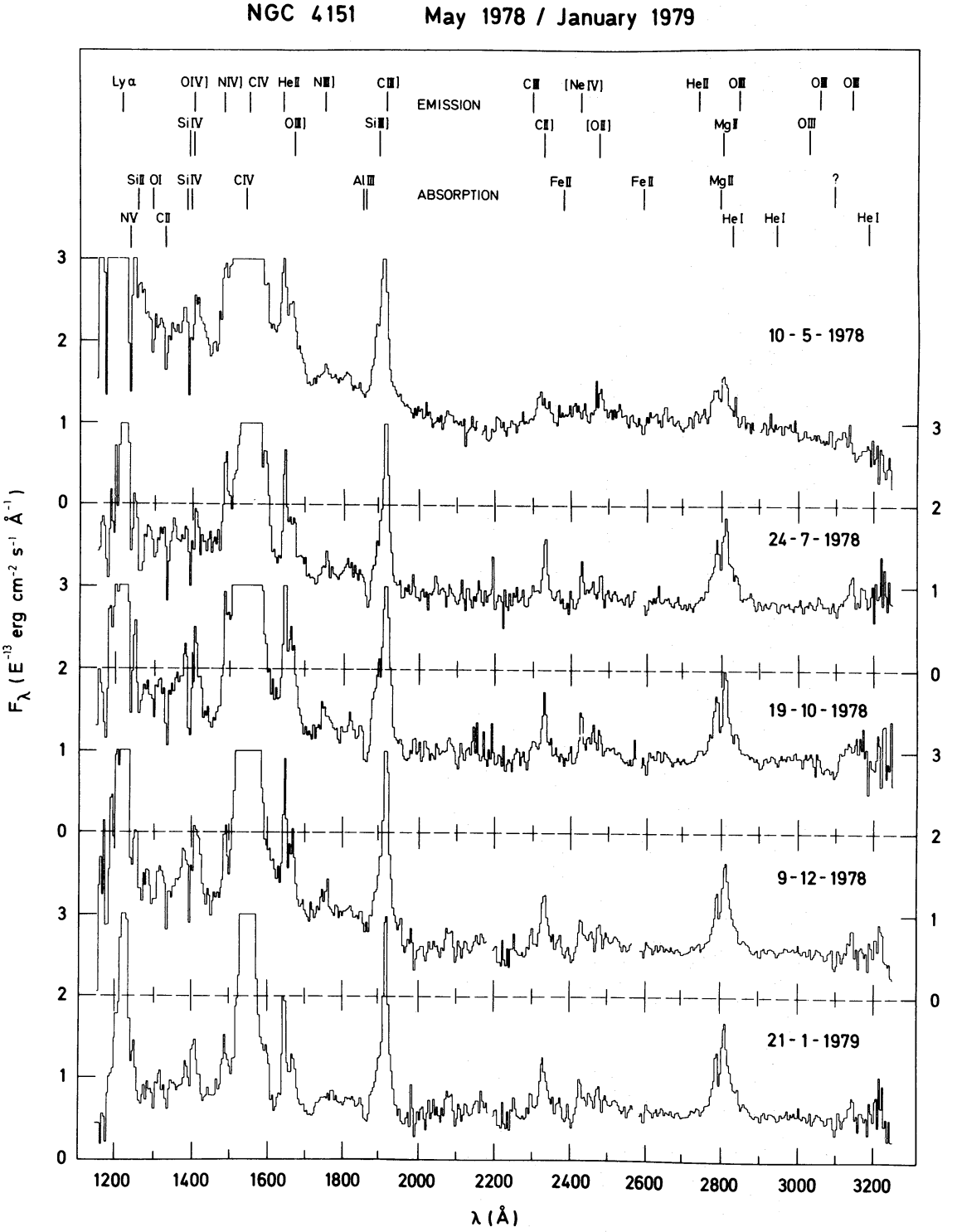

Figure 2. Montage of combined short and long wavelength spectra of NGC 4151 from the first year of *IUE*.

the wavelengths of selected emission lines to coincide with their predicted positions assuming $z = 0.0033$. Unfortunately, the absorption lines cannot be used as they may be blends of a broad component formed in NGC 4151, and two narrow components, one formed in the Galaxy and one in NGC 4151. Neither can strong permitted resonance lines be used; they have both absorption and emission components. This leaves very few suitable features. In the LWR spectra the O III line at λ 3133, the C II] λ 2326 and C III] λ 1908 lines were used

and for the SWP spectra, the He II λ1640 and C III] λ1908 lines. Even these C II] and C III] lines are in fact blends whose precise wavelengths are density-sensitive (Nussbaumer & Schild 1979), whilst the He II line has a weak absorption component superimposed on its blue wing (Penston *et al.* 1979).

After the wavelength scale was determined for each spectrum, data obtained on the same day were averaged and regions affected by saturation, fiducials, geocoronal Lα emission and particle events were excluded from the mean spectra. Large aperture spectra were given equal weight and small aperture spectra a weighting factor proportional to the ratio of large to true small aperture exposure times (true exposure time = nominal exposure time × aperture transmission).

In the overlap region between long and short wavelength camera images, LWR data for $\lambda > 1925$ Å, large aperture SWP spectra for $\lambda < 1950$ Å and small aperture SWP results for $\lambda < 1975$ Å were used. For the data presented in this paper there is good agreement between the C III] (λ1908) line strength as measured from long and short wavelength camera images.

The final spectra are shown in Figs 1 and 2. The wavelength scale in the short wavelength region is good to at least half a wavelength bin (1.3 Å). In the long wavelength region it depends both on the accuracy of the adopted reference wavelengths ($\lesssim 2$ Å) and the accuracy of the IUESIPS dispersion constants. The latter may be the limiting factor since there is evidence from spectra of galactic objects with many narrow emission lines that discrepancies between C II] λ 2326 and O III λ 3133 occasionally can be some 4 or 5 Å.

2.3 PHOTOMETRIC ACCURACY AND REPEATABILITY

In the study of the ultraviolet spectrum of NGC 4151 the most striking aspect is the variability of both lines and continua. For the analysis of these phenomena a reliable estimate of the repeatability of the data is crucial and the absolute photometric accuracy is actually of lower importance.

Unfortunately no overall estimate of the repeatability for the whole of these first-year data can be given. The performance of the scientific instrument improved considerably during this period and the selection of the optimum combination of exposure times for observing NGC 4151 was not finished until 1978 October.

The 1978 May spectrum is of lower quality in this respect: no large aperture data were obtained and a wide range of exposure times were tried (Table 1) resulting in seriously under- and overexposed parts of spectra. Reduction of these spectra also used the original, noisier ITF. The mean spectrum in this case was constructed from different parts of the various spectra resulting in a final spectrum of rather inhomogeneous quality. The region shortward of λ1200 is better than normal due to the inclusion of SWP 1518 with its very long exposure time. The scale factor obtained from the C III] + Si III] feature has an estimated 10 per cent uncertainty, and the possible photometric errors in this spectrum may be up to 20 per cent. In addition, the wavelength scale for the May data is less accurate than is normal for SWP data (± 2.5 Å) probably on account of both the inferior early IUESIPS dispersion constants and the fitting together of many separate pieces of spectrum.

The 1978 February data have a different flux calibration (Snijders 1979) from all later data (Bohlin *et al.* 1980) but the two calibrations were obtained using identical methods and have calibration targets in common (Snijders 1979). The major source of errors is the scaling of the absolute flux level from the C III] + Si III] feature, for which a 10 per cent accuracy is again estimated. This scaling factor is 0.85 (that is, the flux estimates of Boksenberg *et al.* (1978) for NGC 4151 on February 28 are 15 per cent too high), in good agreement with earlier estimates of the variations in large aperture transmission in the commissioning phase (Boksenberg *et al.* 1978; Snijders 1979). The spectrum could have photometric errors as large as 15 per cent but more likely they are a factor of 2 smaller.

These February and May data then appear brighter than most spectra in the present data set, but have similar continuum flux levels to those of later (1979 May and June) data. This result is supported by the fact that the N v absorption also had similar strength in these epochs, as expected from the general correlation of continuum flux and high-excitation absorption lines discussed in Section 6.3.

For the more uniform data obtained after 1978 May, comparison of mean fluxes in 50 Å bins yields rms differences between spectra taken on the same date that suggest repeatability to better than 5 per cent in the well-exposed parts of the spectra.

3 The continuum

3.1 CHOICE OF CONTINUUM POINTS AND FORM OF SPECTRUM

The selection of a sufficient number of spectral intervals apparently free from both emission and absorption lines is relatively easy in the long wavelength region ($\lambda > 2000$ Å). The regions chosen are listed in Table 2. The data for the four dates on which spectra in both wavelength ranges were obtained in the large aperture, are displayed in Fig. 3 as plots of $\log f_\nu$ against $\log \nu$. The data of 1978 May obtained in the small aperture are basically similar. The estimated error on each point is of order ±5 per cent. Despite variations in intensity the flux distributions in the interval λλ3000–2000 (15.0–15.18 in $\log \nu$) are similar at each epoch, approximately following a power law $f_\nu \propto \nu^\alpha$ with α in the range -1.7 to -2.0.

By contrast, in the short wavelength region ($\lambda < 2000$ Å) the location of the continuum points is much more troublesome. Five such candidate regions, all narrow, are listed in Table 2. The point at 1865 Å is a rather sharp minimum and it is at least partially attributable to absorption by Al III λλ1855, 1863: for this reason it is bracketed in Fig. 3. The point at λ1705 is also a minimum but no acceptable explanation in terms of absorption could be found. Between these two minima the spectra show a plateau on which were selected the two candidate regions at λ1800 and λ1735. The last point, at λ1455, is situated between the medium-strength emission features of N IV] and O IV]/Si IV. Shortward of λ1400, there are many crowded emission and absorption lines so that no convincing continuum windows could be found.

There are two alternatives. The first is a 'high' continuum passing through the points at λλ1800, 1735 and 1455. This continuum bends sharply around λ2000 ($\log \nu = 15.2$) to a

Table 2. Continuum regions chosen.

Central wavelength (Å)	Wavelength range (Å)	Comment
3020	40	
2902.5	35	
2705	30	
2675	30	
2415	10	
2225	50	
2165	70	
2055	150	
1865	10	Al III absorption
1800	10	Unidentified emission?
1735	10	Unidentified emission?
1705	10	Preferred
1455	30	Preferred

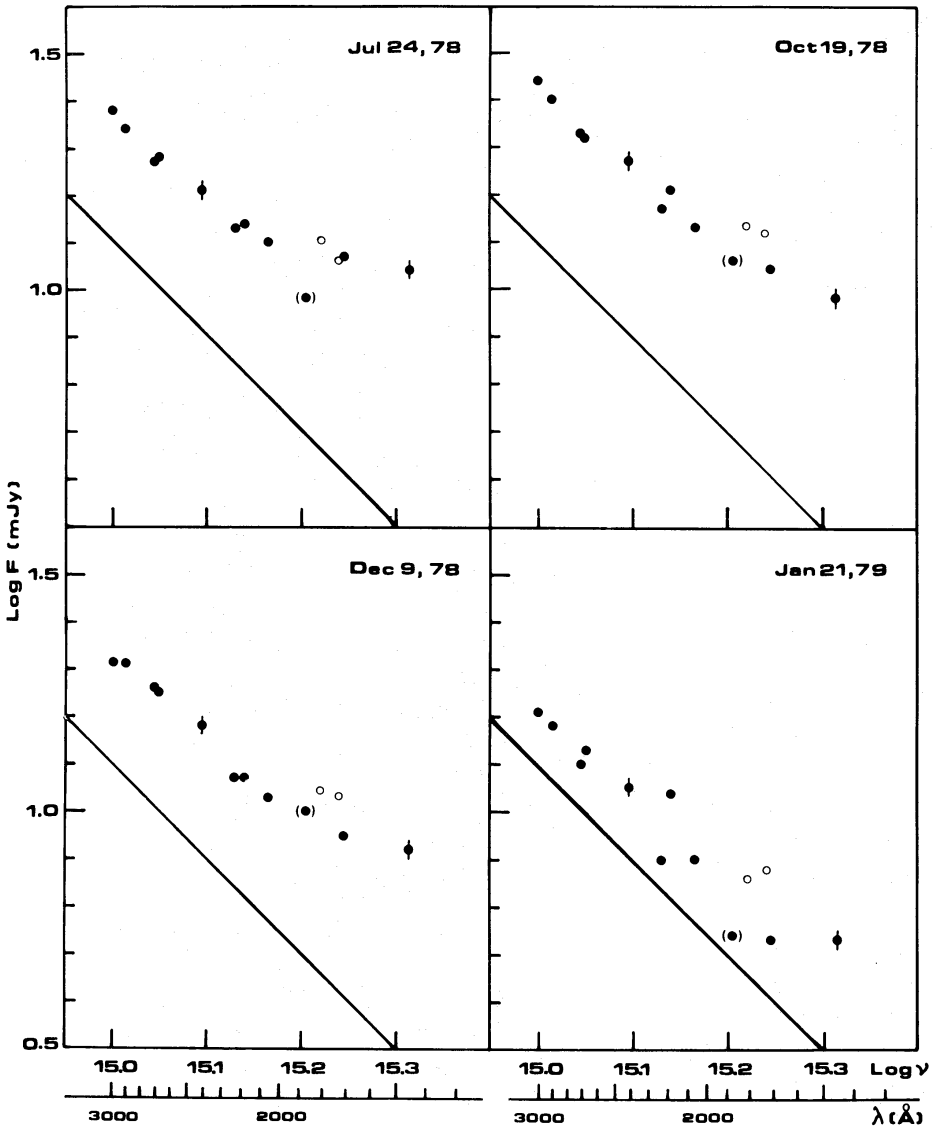

Figure 3. Ultraviolet continuum energy distributions of NGC 4151 at four different epochs. The choice of continuum points is discussed in the text and preferred continuum points appear as unbracketed closed symbols – the bracketed point is contaminated by Al III λ1862 absorption and open symbols are suspected to be on emission features (see text). Error bars appear unless they would be smaller than the plotted symbols. The solid line is present in each quarter of the figure in the same place to guide the eye. Note the changes of level and shape.

slope near zero and turns down again to higher frequencies. With this choice the dip at λ1705 lacks an explanation. Alternatively, one may choose to put a 'low' continuum through λ1705 and λ1455. Then the plateau is seen to represent a blend of emission lines one of which emerges in some spectra and is identified as N III] λ1750. There is more discussion of this point in Section 5. It is interesting that at some epochs the low continuum passes close to the λ1865 point suggesting that any Al III absorption is weak on these occasions. We prefer the generally smoother nature of the low continuum and the concept that unidentified emission lines are more likely than unidentified absorptions (which would have to be permitted lines from ground or low-lying metastable states and thus be more likely to appear in wavelength lists). The λ1705 and λ1455 points are therefore shown as closed symbols in Fig. 3, while those at λ1800 and λ1735 are open circles.

Table 3. Characteristics of least-squares fits to long-wavelength continuum points, and excess flux over this fit at 1455 Å

Date	Flux at 2500 Å (10^{-14} erg cm^{-2} s^{-1} Å^{-1})	Spectral index	Excess at 1455 Å (10^{-14} erg cm^{-2} s^{-1} Å^{-1})
1978 May	11.3 ± 0.2	−1.95 ± 0.14	11.6 ± 1.0
July	8.2 ± 0.1	−1.67 ± 0.08	5.6 ± 0.6
Oct	9.2 ± 0.1	−1.74 ± 0.12	2.9 ± 0.8
Dec	7.3 ± 0.1	−1.84 ± 0.11	3.8 ± 0.6
1979 Jan	5.4 ± 0.1	−1.97 ± 0.17	2.2 ± 0.6

The preferred low continuum shows a gradual flattening toward higher frequencies near λ 2000 (log $\nu \sim 15.2$) suggesting that the ultraviolet continuum can be decomposed into two components. The long wavelength component seems to have fairly constant slope with α near −2 (without correction for interstellar reddening). The short wavelength component is flatter. The ratio of the flux at 1455 Å to the extrapolation of the long wavelength power law seems to vary significantly from epoch to epoch, suggesting that the forms of the variation of each component are not exactly synchronous.

Evidence for a two-component picture of the continuum emission from the nucleus of NGC 4151 is also provided by results on optical polarization (Thomson *et al.* 1979; Schmidt & Miller 1980). A polarized component with $\alpha = -0.3$ is found in the optical region, and may be related to the flat short wavelength component proposed here.

To investigate further the properties of these two continua, and noting that the short wavelength component is only defined by the two continuum points at λ1705 and λ1455, the following procedure was adopted. A power law was fitted to the long wavelength continuum points (λ > 2000 Å) and the flux read off at λ 2500 to define the long wavelength component. Then the extrapolated value predicted by this power law at λ1455 was subtracted from the observed value at that point to give an excess attributed to the short wavelength component. The results are presented in Table 3 for $E(B-V) = 0.00$. Similar fits were made after correction for interstellar reddening appropriate to $E(B-V) = 0.05$ mag (see Section 3.2). In this latter case however, the short wavelength excess, while present in 1978 May and July, is neglibly small for 1978 October, December and 1979 January. Taken at face value these results suggest that the variations of long and short wavelength components are different, as may also be visually apparent in Fig. 3.

3.2 CORRECTION FOR INTERSTELLAR REDDENING

There is little evidence of any smooth depression near λ 2200 Å attributable to dust absorption. It is therefore questionable if any reddening correction should be applied. To test this the data were adjusted for various values of $E(B-V)$ using the extinction formulae given by Seaton (1979). As an example, the results for the 1978 December data are illustrated in Fig. 4.

The largest correction corresponds to $E(B-V) = 0.24$ mag, a value inferred for the narrow-emission-line region using [S II] lines (Wampler 1971). The spectrum then takes on a very peculiar shape with a strong peak at λ 2200, suggesting the reddening is overestimated. We conclude that the ultraviolet continuum source is seen unobstructed through the system of clouds and filaments, which must contain their own dust, occupying the 100 pc diameter narrow-line region.

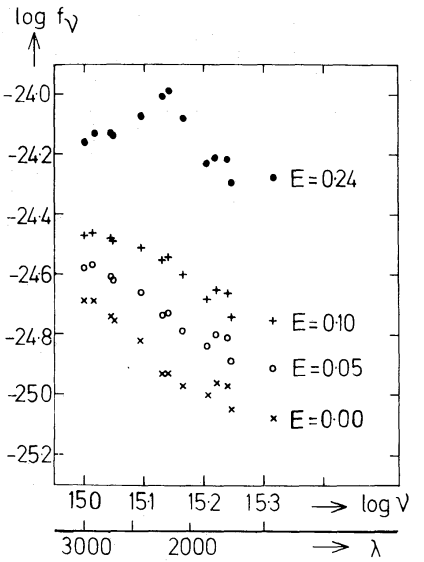

Figure 4. Results of various trial dereddenings applied to the NGC 4151 continuum of 1978 December. The bottom crosses represent the observed data. Open circles, pluses, and closed circles represent $E(B-V)$ values of 0.05, 0.10 and 0.24 mag respectively. It appears the reddening lies between 0.05 and 0.10 mag.

The smallest correction corresponds to $E(B-V) = 0.05$ mag, which is a conservative lower limit expected from dust in our own Galaxy at a latitude of 75°. Here the 'low' continuum points retain the same general shape, suggesting a power law with $\alpha = -1.1$ to -1.5 longward of λ2000 (log $\nu \sim 15.2$) and a flattening shortward, particularly noticeable by the shortest wavelength point at log $\nu = 15.31$.

An intermediate value of $E(B-V) = 0.10$ mag, also presented in Fig. 4, has the virtue of making the connection of the 'high' continuum and long wavelength points rather smooth but leaves a noticeable bump at λ2200 and the problematical minimum at λ1705. The reddening in the interstellar medium of NGC 4151 is certainly no greater than it is in our own Galaxy. The limit $E(B-V) < 0.1$ agrees with the *ANS* results of Wu & Weedman (1978) and the commissioning value $E(B-V) = 0.06$ of Boksenberg *et al.* (1978).

3.3 RELATIONSHIP TO OTHER WAVEBANDS

Fig. 5 presents the electromagnetic spectrum of NGC 4151 from a representative collection of measurements, from the radio to the MeV region. For the infrared and visual regions, where the source is variable, only sets of typical data are shown. For the infrared, the results given in Rieke (1978) are plotted. These form a homogeneous set from 1.25 to 34 μm and indicate a possible turnover around 20 μm. For the visual wavelengths the results given by de Bruyn & Sargent (1978) are used. In this region the hump shortward of λ4000 is due to Balmer continuum emission (Boksenberg *et al.* 1978). The small discrepancy between infrared and visual data is probably due to a combination of source variability and the use of a slightly larger aperture for the optical than the infrared measurements (10 versus 5.5 arcsec or less). This dependence of measured flux on aperture size due to contamination by starlight is clearly demonstrated in the results of Penston *et al.* (1974).

For the ultraviolet region the highest and lowest continua from Fig. 3 are shown. For the X-ray region, a sketch is reproduced from the composite spectrum given in Perotti *et al.* (1979). Note the variable cut-off at low X-ray energies, which is attributed to a changing column density of absorbing gas. The intensity is known to be highly variable up to 20–30 keV, but the best-fit power law slope appears to remain constant, $\alpha \simeq -0.45$ (Mushotzky *et al.*

1978, 1980). A flattening is evident above 30 keV, where the spectrum maintains a slope of almost zero up to about 3 MeV, and then drops. However, recent observations above 100 keV and up to 20 MeV (Meegan & Haymes 1979; White *et al.* 1980) have yielded upper limits in conflict with the previous measurements (see again Fig. 5 where two representative limits are also given) indicating either a variation in the source strength or a much steeper spectral slope above 100 keV than had been previously thought. Most of the power from NGC 4151 comes from very hard X-rays.

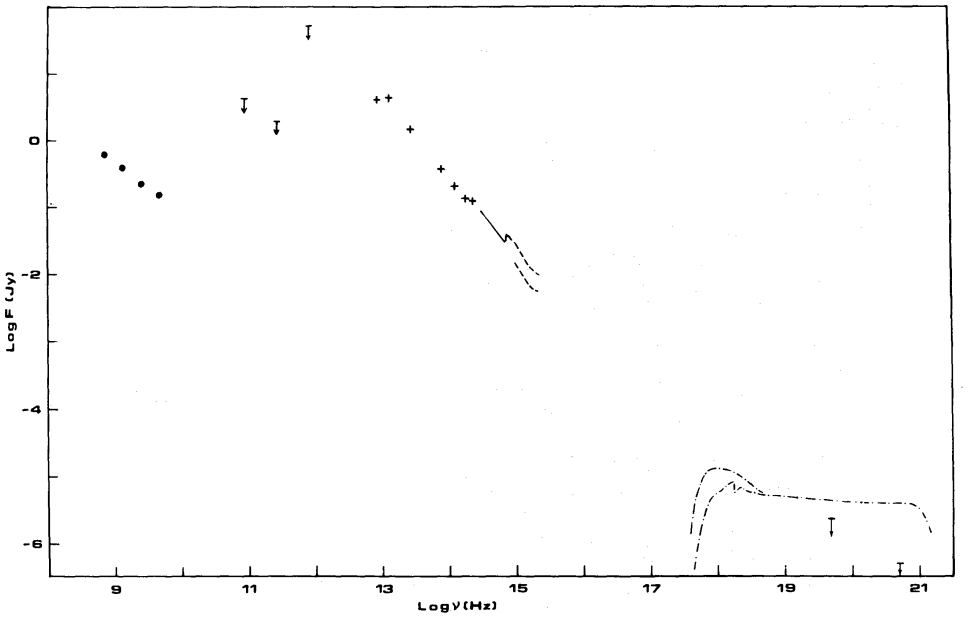

Figure 5. Overall continuum electromagnetic spectrum of NGC 4151. Radio data from Kellerman & Pauliny-Toth (1968), van der Kruit (1971), de Bruyn & Willis (1974) and Sramek (1975). Microwave upper limits from Elias *et al.* (1978), Fogarty *et al.* (1971) and Hudson & Soifer (quoted by Baity *et al.* 1975). Optical data from de Bruyn & Sargent (1978). UV data from this paper, the highest and lowest continua from Fig. 3, are plotted. The X-ray spectrum is sketched from the collection of data by Perotti *et al.* (1979) with two representative upper limits beyond 100 keV (Meegan & Haymes 1979; White *et al.* 1980).

Lacking simultaneous observations in the optical and ultraviolet bands for the present study, only spectral shapes can be compared here. The optical continuum (Fig. 5) can be represented by a power law with a spectral index -1.4, which is less steep than that now measured in the $\lambda\lambda$ 2000–3000 Å band. However, when a reddening correction corresponding to $E(B-V) = 0.05$ is applied, the two spectral indices become approximately the same, about -1.2, indicating that the ultraviolet continuum deduced from the long wavelength *IUE* range is an extrapolation of the optical continuum. The distribution of infrared points (Fig. 5) suggests a single component contributing a power law spectrum with (approximately) constant slope from $\sim 10^{13}$ to 1.5×10^{15} Hz. Its extrapolation to 10^{18} Hz gives a flux comparable with that actually observed. This might be just a coincidence, and the component that is seen to emerge around 2×10^{15} Hz may be more closely connected with the X-ray emission. Unfortunately, the gap between the high frequency end of the *IUE* range and the soft X-ray observations is hardly likely to be bridged by direct observations in the near future, and this emphasizes the importance of simultaneous monitoring of variability in the two domains.

4 Absorption lines

4.1 EQUIVALENT WIDTHS AND RELATIVE WAVELENGTHS

The generally good signal-to-noise ratios of the present data, achieved by averaging several spectra, enable the number of positively identified ultraviolet absorption lines to be increased compared with the lists of previous investigators (Davidsen & Hartig 1978; Boksenberg *et al.* 1978). In columns 1 and 2 of Table 4 are listed the atomic transitions which are likely to be the major contributors to 14 of the absorption features detected. The data in the table do not include measurements of the Lyman α absorption line, which cannot be separated from the corresponding emission in *IUE* low dispersion spectra, nor of He II λ1640, which has been detected in *IUE* high resolution spectra of NGC 4151 (Penston *et al.* 1979) but is too weak to be identified with certainty at the lower resolution of the present data. The values quoted for λ_{lab} are vacuum wavelengths of the resonance lines within each multiplet, and were taken from the compilation of Morton & Smith (1973). The only exception is C III λ1175.7, which arises from the metastable $2s2p\ ^3P^o$ term (Noerdlinger & Dynan 1975). In Table 4 are also given values of equivalent width W_λ, and wavelength shift $\Delta\lambda$ ($=\lambda_{obs}-\lambda_{lab}$) measured for the 14 absorption features from the averaged spectra of Fig. 1. These data were obtained using the expressions:

$$W_\lambda = \sum (1 - F_i/F_c)\,\delta\lambda_i$$

and

$$\lambda_{obs} = \sum \lambda_i (1 - F_i/F_c)\,\delta\lambda_i / \sum (1 - F_i/F_c)\,\delta\lambda_i,$$

where F_i and F_c are the values of flux respectively in the line and in the local continuum, at the wavelength λ_i of the ith sampling bin; and $\delta\lambda_i$ is the bin width. The summations were carried out over an interval judged subjectively to span the full extent of an absorption feature.

As discussed in Section 2.2, the wavelength scale to which the values of λ_{obs} refer was obtained by forcing the wavelengths of selected emission lines to agree on each individual image with the values expected from the optical emission line redshift of NGC 4151 (z = 0.0033 in a heliocentric frame of reference). Consequently there may be small systematic errors in the absolute wavelength scale of each averaged spectrum. Additionally, the determination of the central wavelength of the lines is sensitive to the choice of continuum level, when this is sloping (see Table 4). An indication of the random error appropriate to the values of λ_{obs} follows from consideration of the Si IV doublet lines which are resolved and unlikely to be blended with other features. The data in the table show that the two values of $\Delta\lambda$ for this doublet measured on the same date do not differ by more than 0.7 Å, which is slightly more than one quarter of a sampling bin in the SWP images (for the LWR data one bin is approximately 4.5 Å). However, zero point errors in SWP mean spectra, which differ from day to day, roughly double the possible errors in the absolute wavelength scale to 0.5 sampling bin. Furthermore, weaker lines intrinsically may have larger errors. No wavelength measurements are given for the 1978 May spectra, because of greater uncertainties in the reduction process (see Section 2.3).

In general, accurate measurement of the equivalent widths of the absorption lines in these spectra is difficult. For the averaged spectra of Figs 1 and 2 the probable errors in W_λ due to statistical fluctuations in the signal are typically between 10 and 50 per cent, depending on the quality of the data. Values of W_λ measured from individual images prior to averaging were found to deviate from the mean by comparable amounts. A more serious problem arises from the frequent blending of absorption and emission features (see Fig. 1) which

Table 4. Absorption line equivalent widths and relative wavelengths.

Ion	λ_{lab}	1978 Feb 28		1978 May	1978 July 24		1978 Aug 2		1978 Oct 19		1978 Dec 9		1979 Jan 21	
		$\Delta\lambda$	W_λ	W_λ	$\Delta\lambda$	W_λ	$\Delta\lambda$	W_λ	$\Delta\lambda$	W_λ	$\Delta\lambda$	W_λ	$\Delta\lambda$	W_λ
C II	1334.5	+2.3	3.0	2.0	+2.3	3.1	+1.6	3.6	0.4–0.2	2.4–2.8	2.1–2.0	2.5–3.0	+0.5	2.6
C III*	1175.7	+0.5	4.0	4.0	+2.7	3.1	−0.6/−0.2	7.2–8.7	−0.5/−0.8	2.3–5.1	2.6–4.0	3.4–6.6	+0.4/−1.1	4.2–5.5
C IV	1549.1	+0.9	⩾3.0	⩾3.8	+1.1	⩾2.7	−0.2	⩾2.4	0.0	⩾3.5	+2.3	⩾3.1	−0.1	⩾2.3
N V	1240.1	1.4–5.8	⩾6.0	⩾7.0	⩾2.2	⩾2.4	+1.5	⩾2.9	+2.7	⩾4.0	+4.0	⩾2.1	+2.0	⩾2.1
					+1.4	⩾3.7			+1.4	⩾5.2			+1.1	⩾3.4
Mg II	2797.9			2.2	−0.6:	2.5–3.7			−1.3	⩾3.9	−0.4/−0.1	3.1–3.7	0.0/−0.8	2.9–4.8
Al III	1857.4	:	2.0:	1.2	+6.5	4.3–5.2	4.3–4.7	2.5–4.1	3.0–3.3	2.9–4.2	+5.9	3.0	+0.7	4.2
Si II	1526.7	present?		0.8	present		0.3–2.9	1.0–1.6	⩾0.8	⩾1.1	present		:	1.3:
Si II–O I	1303.3	present?		1.6	+0.4	0.7–1.5	−1.7	1.2	−2.8	1.4	−2.1	3.5:	−3.0	1.9
Si II	1260.4	present		0.8	+6.1	3.4–5.3	+2.9	4.6	4.2–3.0	1.9–3.5	7.3–6.5	2.2–3.8	4.4–2.8	3.0–4.9
Si II	1191.9	:	1.0:	1.3	+3.6	2.0	fiducial		+0.9	1.5	+5.7	1.7	fiducial	
Si III	1206.5			present	⩾0.3	⩾1.5	geocoronal Lyα		+0.1	⩾0.8	+3.7	1.4:	geocoronal Lyα	
Si IV	1402.8	:	1.5	1.6	+0.8	2.1	0.0	1.8	+0.4	2.5	+1.6	1.7	⩽0.8	0.6:
Si IV	1393.8	:	3–5	3.3	+1.5	3.7	+0.4	4.4	−0.3	5.0	+2.1	3.8	⩽1.1	2.2:
Fe II	2599.4			1.9	+1.1:	1.5			−0.1	1.7	+1.7:	0.8	−3.7	1.5

Notes: $\Delta\lambda$ and W_λ are in Å. $\Delta\lambda = \lambda_{obs} - \lambda_{lab}$, where λ_{obs} is measured on a wavelength scale determined by positions of unblended emission lines at the appropriate redshift. λ_{lab} values do not include possible contributions from fine structure lines. A full discussion of errors associated with the measurements is given in the text, (Section 4.1).

often precludes an unambiguous estimate of the local continuum. In most cases it was possible to determine likely minimum and maximum values of the local continuum flux using respectively a straight line and a polynomial to interpolate between portions of an emission line adjacent to an absorption feature. The corresponding limits to W_λ are listed separately in Table 4, unless the range in W_λ is less than ±20 per cent, in which case a single average value is given. The lines most severely affected by this problem are those which are blended with the strongest emission features, for example, C IV λ1549.1 and Si II λ1526.7 which occur respectively near the core and in the blue wing of C IV emission, and N V λ1240.1 and Si II λ1206.4 which are found in the wings of Lyman α. Often for these lines only a conservative lower limit to W_λ is quoted, corresponding to the minimum value of the local continuum (linear interpolation). It is important for the later discussion on variability (Sections 4.3 and 6) to understand that variations in these lower limits between different epochs correspond to real changes in the overall spectrum, although it is inherently difficult to measure separately the absorption and emission line contributions to the change of a feature (see Fig. 1). The extent to which the measures are affected by these problems varies from spectrum to spectrum, reflecting changes both in the quality of the data and intrinsically in NGC 4151. Consequently, apparent inconsistencies in Table 4 indicate various degrees of difficulty in the measurements.

Finally, a more fundamental obstacle in the derivation of useful equivalent widths is the currently poor knowledge of the geometry of the nuclear regions of NGC 4151. This is required to convert the measured

$$W_\lambda = \sum (1 - F_i/F_c)\, \delta\lambda_i$$

into the physically meaningful quantity:

$$W'_\lambda = \int [1 - \exp(-\tau_\lambda)]\, d\lambda,$$

where τ_λ is directly proportional to the column density N of absorbers. In general (Anderson 1974) W_λ is smaller than W'_λ by a factor depending on the proportions of the continuum and emission line fluxes covered in line of sight by the absorption line region. The high resolution profiles of the C IV and Ly α lines (Penston *et al.* 1979) argue in favour of almost complete coverage of the broad-line emission region between −100 and −1100 km s^{-1} (with respect to the narrow-line redshift), but little can be inferred concerning the location of the absorbing gas relative to the region producing the ultraviolet continuum. The importance of this point is emphasized by the recent X-ray spectrum of NGC 4151 by Holt *et al.* (1980) which indeed shows that the X-ray source is only 90 per cent covered by the material causing the photoelectric absorption at those wavelengths. However, it is hard to draw firm conclusions for the ultraviolet since it is not yet known if the X-ray and ultraviolet emission or absorption regions are co-extensive. Consequently, quite apart from the problems in the measurement of the line strengths discussed above, the values of W_λ given in Table 4 are lower limits of the equivalent widths of the corresponding absorption lines.

4.2 VELOCITY CONSIDERATIONS

The absorption lines in the spectrum of NGC 4151 will mainly be formed in three distinct regions:

(i) the disc and halo of our Galaxy;
(ii) the general interstellar medium of NGC 4151; and
(iii) the nucleus of NGC 4151.

While those arising in region (ii) will be close to the emission line redshift of NGC 4151 (960 km s^{-1}), absorption from regions (i) and (iii) will overlap in velocity, since the redshift range of the latter is approximately -100 to $+900$ km s^{-1} (Anderson & Kraft 1969; Penston *et al.* 1979). Available optical and ultraviolet data, however, suggest that lines from region (iii) may be stronger because of the greater velocity range, that they may be variable, and may include a wider range of ionization and excitation states.

The vast majority of the values of $\Delta\lambda$ in Table 4 show a net blueshift relative to the emission line region, of between 300 and 1000 km s^{-1} ($\Delta\lambda/\lambda$ in the range $1.0\times10^{-3}-3.5\times10^{-3}$), a value consistent with their origin in the nucleus of NGC 4151.

Two features which depart from the general pattern are Si II λ1260.4 and the Si II/O I blend near λ1303. Both can be understood in terms of blending with other lines. The former appears red-shifted by 2–3 Å relative to Si II λ1191.9, suggesting a significant contribution to the absorption by λ1264.7, the strongest Si II fine-structure line. (The fine-structure transitions in the λ1191.9 multiplet would give a smaller shift, being weaker and closer to the resonance lines (Nussbaumer 1977).) In contrast the feature near λ1303 is blue-shifted by 4–6 Å more than Si II λ1191.9, and is anomalously strong relative to other Si II lines, indicating that Si III λ1298.9 may be an important contributor. This line arises from the extremely metastable $3p\ ^3P^0$ levels: the lower excitation potential and the transition probability of this line are comparable to those of the analogous transition in C III at λ1175.7 (Noerdlinger & Dynan 1975) which is very strong in our spectra. Finding that lines from metastable levels contribute significantly to the λ1260 and λ1303 blends is in agreement with the known degree of excitation of the optical and ultraviolet spectrum. In addition, the Al III λλ1855, 1863 blend lies at a somewhat high $\Delta\lambda$. Although this could be due largely to saturation effects giving a smaller doublet ratio than the 2:1 value assumed to compute the reference wavelength, a similar shift to positive velocities seems to occur in the individual Al III lines seen at high dispersion (Penston *et al.* 1979).

Direct examination of the $\Delta\lambda$ values in Table 4 shows that time variations in the relative velocity of emission and absorption are of only marginal significance. Possibly the velocity difference was lower on 1978 August 2 and December 9, but the reality of these effects is doubtful. More convincing and sensitive evidence of time variations in the velocity of the outflowing gas is provided by a direct comparison in Fig. 1 of the C IV and Si IV composite emission and absorption profiles at difference epochs. The intensity ratio of the shorter λ to longer λ ('violet' to 'red') peaks of the emission lines (the V/R ratio – given in Table 5) was clearly at a maximum on 28 February 1978, decreased to a minimum on 1978 July 24 and subsequently remained at this lower value. The implied variability of the velocity difference

Table 5. Variations of the C IV ratio at the epochs of observation. V/R is the ratio of the shortward to longward emission peak intensities above the adopted continuum.

Date	V/R
1978 Feb	1.08
May	0.91
July	0.66
Aug	0.69
Oct	0.69
Dec	0.75
1979 Jan	0.69

between absorption and emission lines may be more rapid than our sampling frequency. In fact, rapid variations of the profiles of the C IV and Si IV lines are indicated by later spectra obtained in 1979 May and to be discussed in forthcoming papers.

4.3 VARIATIONS IN LINE STRENGTHS

With the present resolution, changes in the strengths of the absorption lines can be more easily measured than can velocity fluctuations. Table 4 shows that the line strength measures for Si IV and the lower limits for C IV and N V vary together. As noted in Section 4.1, changes in these lower limits correspond to real *changes* in the corresponding line profiles which *may* be attributed to changes in absorption. By contrast, the lines of lower ions show generally smaller variations. The most plausible changes are in Al III λ1857.4 and Si II λ1260.4 which are possibly anti-correlated with those of higher ionization species. In Section 6 these variations are related to those of the ultraviolet continuum and are discussed further.

4.4 COLUMN DENSITIES

As pointed out by Mushotzky *et al.* (1978) there is an apparent discrepancy between, on the one hand, the low dust column in line to the nucleus of NGC 4151 implied by the continuum reddening and, on the other hand, that expected considering the large gas column absorbing the X-ray flux. Assuming a normal reddening law, the form of the ultraviolet continuum near 2200 Å places an upper limit on the colour excess, $E(B-V) \leqslant 0.1$ (Boksenberg *et al.* 1978; Section 3 of this paper). By contrast, the lowest X-ray column deduced ($N_{\rm H} = 2 \times 10^{22}$ cm^{-2}: Ives, Sanford & Penston 1976) would imply $E(B-V) \simeq 3.5$ if the gas-to-dust ratio in the X-ray absorbing region were comparable to the mean value in the solar neighbourhood (Bohlin, Savage & Drake 1978) and the reddening law in NGC 4151 were again the same as the standard galactic one (e.g. Seaton 1979). One possibility is that the gas-to-dust ratio appropriate to the X-ray material is two orders of magnitude greater than the local value. Similar dust deficiencies have been reported for galactic H II regions (e.g. Gillett *et al.* 1975). Alternatively, the apparent discrepancy may be due to a geometrical effect, with the source of the ultraviolet continuum being only partially obscured by the X-ray absorbing region, or being external to it. A clumped distribution of X-ray absorbing 'clouds' of small dimensions relative to the central source size is indicated by recent soft X-ray data (Holt *et al.* 1980).

Clearly, measurements of ion column densities from ultraviolet absorption lines are important in this context. The problem, however, is not completely defined, since a knowledge of the geometry of the nuclear regions of NGC 4151 is required to derive column densities from the observed line strengths, as discussed in Section 4.1. Moreover, it is well known (Nachman & Hobbs 1973) that where several components of different velocity dispersions are blended, as is likely to be the case here, equivalent width data alone can lead to serious underestimates of the total column density of absorbers. Thus, the data of Table 4 can be used at best to place lower limits on the column of gas.

The measurements of Table 4 suggest that throughout the period of our observations the equivalent widths of the resolved Si IV doublet lines remained near the optically thin ratio of 2:1, although the total strength varied substantially. This implies the existence of a broad, unsaturated component with $b > 800$ to $b > 1300$ km s^{-1}, dominating the observed Si IV absorption. (Here $b = \sqrt{2}\,\sigma$, where σ is the equivalent line of sight velocity dispersion). These values are in agreement with the widths of the absorption profiles of C IV and Lyman α measured at high resolution by Penston *et al.* (1979). If a comparable value of b applies to

other ultraviolet absorption lines (this assumption is consistent with the observed line profiles) we obtain a lower limit for the sum of the column densities due to different ionization and excitation stages of silicon:

$N(\text{Si II} + \text{Si II}^* + \text{Si III} + \text{Si IV}) > 3.3 \times 10^{14}\ \text{cm}^{-2}$.

This result refers to the measurements of 1978 August when the cumulative column densities were at a maximum. This value actually underestimates the lower limit to N(Si), as there is no allowance for unobserved ionization and excitation states. With the further assumption of a solar abundance ratio Si/H ($= 3.55 \times 10^{-5}$: Morton 1978) the limit $N(\text{H}) > 3.0 \times 10^{19}\ \text{cm}^{-2}$ is obtained. (Note that available estimates of heavy element abundances in the nuclear regions of NGC 4151 are within a factor of 2 of solar values (Barr *et al.* 1977; Mushotzky, Holt & Serlemitsos 1978; Holt *et al.* 1980).) Applying similar considerations to the observed C lines, $N(\text{H}) > 1.2 \times 10^{19}\ \text{cm}^{-2}$ is deduced. Other elements give even smaller lower limits, because of the paucity of absorption lines available. However, model calculations show that narrow components with much higher column densities can be 'hidden' in the line profiles at the present resolution. For example, if components with b values in the range 20 to 50 km s^{-1} and total gas column densities $N(\text{H}) \simeq 5$–$10 \times 10^{22}\ \text{cm}^{-2}$ (consistent with the X-ray absorption) did occur near the middle of the velocity range covered by the broad region with $b \sim 10^3$ km s^{-1} and $N(\text{H}) \simeq 3 \times 10^{19}\ \text{cm}^{-2}$, the resulting line profiles would be essentially indistinguishable from those produced by the broad region alone. Consequently, the present data cannot yield an unambiguous estimate of the gas-to-dust ratio in the absorption line region. Since the ultraviolet lines alone do not require such a large column as does the strong X-ray absorption, the implication contained in the discussion of Davidsen & Hartig (1978), namely that their C II and Si II absorption equivalent widths (comparable to those of Table 4 but obtained with half the resolving power) arise in the X-ray absorbing gas, was premature.

4.5 LOCATION OF ABSORBERS

It is most probable that the variable absorption lines and those from metastable levels are formed primarily in the nucleus of NGC 4151. However, for C II, Mg II, Si II and Fe II, little evidence is available to determine the relative contributions to the absorption lines from the different physical regions in the line of sight. In the cases of C II and Mg II the line strengths exceed, by more than a factor of 2, the values measured in *IUE* spectra of the QSO 3C 273 (Ulrich *et al.* 1980), which refer to a path length through the galactic halo alone. This, however, may be due simply to differences in the distribution of galactic halo gas along the two lines of sight sampled, and does not imply *per se* that the nuclear regions of NGC 4151 contribute to the observed Mg II and C II lines. From the extensive work of de Boer & Savage (1980) and Savage & de Boer (1981) it is evident that the equivalent widths of the Mg II and C II lines formed along different paths through the halos of the Galaxy and of the Magellanic Clouds can differ by more than a factor of 2. However, if the galactic halo corotates with the disc, the material in line to NGC 4151 ($l = 155°$, $b = 75°$), close to the anticentre direction where the differential rotation causes only motions across the line of sight, should be distributed over a narrower range of velocity than that towards 3C 273 ($l = 290°$, $b = 64°$), which lies more nearly parallel to the direction of galactic rotation.

5 Emission lines

5.1 IDENTIFICATIONS AND THEIR IMPLICATIONS

In spite of considerable detailed differences, the most important features of the ultraviolet emission line spectrum of NGC 4151 are similar to those of quasars. There is, for example,

Table 6. Emission line fluxes in NGC 4151 obtained objectively by integrating the observed monochromatic flux less continuum flux in the quoted wavelength range, where continuum is defined by equation (1).

Dominant species	Wavelength range (Å)	Fluxes (10^{-12} erg cm^{-2} s^{-1}) 1978					1979
		May	July	Aug	Oct	Dec	Jan
H I	1200–1240	17.3	15.3		21.0	18.1	14.0
Si IV + O IV]	1380–1440	1.7	0.2	0.5	2.8	2.7	2.0
N IV]	1468–1500	2.8	2.1	3.2	3.4	1.9	1.8
C IV	1500–1634	42.1	26.7	30.5	42.4	38.2	25.4
He II	1634–1655	2.7	1.7	1.9	2.8	2.6	1.8
O III]	1655–1680	2.1	1.0	1.4	2.2	1.8	1.1
N III]	1745–1765	0.3	0.6	0.7	0.8	0.5	0.3
Si III] + C III]	1880–1936	6.4	5.6	6.6	6.9	6.3	5.5
C III	2286–2308	0.2	0.2		0.1	0.3	0.1
[O III] + C II]	2308–2348	0.9	1.1		1.2	1.2	1.1
[Ne IV]	2418–2440	0.6	0.5		0.7	0.7	0.6
O IV?	2440–2471	0.6	0.3		0.7	0.7	0.6
[O II]	2471–2493	1.3	0.3		0.4	0.4	0.4
[Fe XI] ??	2640–2662	0.6	0.1		0.1	0.2	0.1
He II	2719–2750	0.1	0.2		0.2	0.4	0.2
Mg II	2750–2848	5.1	4.9		4.4	5.2	4.6
[A IV]	2848–2879	0.5	0.4		0.3	0.7	0.3
O III	3122–3153	0.2:	1.2		1.0	1.1	0.8

a close correspondence between the lines listed in Table 6 and those given for 3C 273 by Ulrich *et al.* (1980) which, in turn, are found in other quasars observed from the ground (e.g. Baldwin & Netzer 1978).

Thus the strongest features are the blends of Lyman α with N V λ1240, and Si IV λ1398 with O IV] λ1402, and multiplets of C IV λ1549, He II λ1640, O III] λ1663, C III] λ1909, C II] λ2326 and Mg II λ2800. In contrast to quasars, however, it is apparent from inspection of Fig. 1 that the line profiles are not all the same, as has been found by Penston *et al.* (1979) from high dispersion shortwave data. In part this is caused by absorption effects which make Lyman α and He II λ1640 sharp and asymmetric and produce reversals in the C IV and Mg II resonance lines. But the narrow cores of C III] λ1909 and C II] λ2325 are also worth noting: presumably a major part of these lines arises in the 'narrow line region' as is also the case for the low density lines of [Ne IV] λ2422 and [O II] λ2470, which are also narrow. Note that another low density line [O III] λ2320 may contribute to the C II] feature.

Other features that are present but either weaker or blended include N IV] λ1486, N III] λ1750 and Si III] λ1892 in the shortwave region. In the longwave region the C III line at λ2296 is apparent and represents its first detection in an active extragalactic object. The O III Bowen lines, notably λ3133, and He II Paschen series members λλ3203 and 2733 are also distinguishable. Longward of λ3100, the *IUE* data overlap with the ground-based results of Boksenberg & Penston (1976) and show the same strong features.

When one attempts to push the line identification procedure to even fainter lines, one encounters considerable difficulties associated not merely with establishing the noise level but also with finding continuum in the presence of combined emission and absorption spectra. In general these problems are less severe in the longwave region but even here one can discern a series of broad low-contrast features underlying the stronger lines.

These are similar to the structures reported by Wills *et al.* (1980) from ground-based observations of quasars, and by Snijders *et al.* (1980) from *IUE* observations of the Fe II galaxies I Zw 1 and II Zw 136. Wills *et al.* attribute these features to Fe II emission. In NGC 4151, the Fe II resonance multiplets (1, 2, 3) are not apparent, but this is understandable in terms of a high opacity in these lines – irrespective of the excitation mechanism. Under these circumstances, as Jordan (1979), Collin-Souffrin *et al.* (1980) and Netzer (1980) point out, the intensity of non-resonance multiplets relative to resonance lines from the same upper levels, is much higher than for the optically thin case. For example, multiplets 60 and 61 may be present, since these share upper levels with 2 and 3 respectively. Other UV multiplets, such as 33 and 34 suggested by Wills *et al.* (1980), may contribute in a similar manner to the NGC 4151 spectrum between λ2400 and λ3000. Whilst Wills *et al.* (1980) and Snijders *et al.* (1980) use 33 and 34 to explain excess flux between λ2400 and λ2550, it should be noted that transitions in these two multiplets have lower oscillator strengths than 60 and 61, and are absent both in the Sun (Burton & Ridgeley 1970) and RR Tel (Penston *et al.* 1981) in spite of the presence of many other Fe II lines. Multiplets 60 and 61 are strong in RR Tel. They lie in a difficult region in the solar specum, where they may be masked, and no firm conclusions can be reached about their presence.

If Fe II UV60 and 61 are comparable in intensity with UV2 and UV3, the implied number of scatterings by the resonance photons is approximately the same as the branching ratio (i.e. $n_{sca} \sim 100$). Now, we have $n_{sca} = \tau_0(\pi \ln \tau_0)^{1/2}$ (Osterbrock 1962) and the optical depth τ_0 is thus ~30. The value of the column density derived from this depends on the velocity dispersion assumed, and for this one can consider two limiting cases. First, one can assume the absorption occurs in individual filaments and the velocity dispersion is as low as the thermal value, $b \sim 10\,\mathrm{km\,s^{-1}}$. Alternatively, an upper limit deduced from the absorption lines can be used, assuming the Fe II self-absorption occurs in an expanding outer layer (i.e. $b \sim 1000\,\mathrm{km\,s^{-1}}$; Penston *et al.* 1979). Probably the former situation is the more plausible. In any case $\tau_0 = 30$ corresponds to a column density $N(\mathrm{Fe^+}) \sim 10^{14.5}\,(b/10)\,\mathrm{cm^{-2}}$ with b in $\mathrm{km\,s^{-1}}$, $N(\mathrm{H}) > 10^{19.5}\,(b/10)\,\mathrm{cm^{-2}}$, assuming solar abundances. The corresponding values implied if UV33 and 34 were in fact of similar strength to the resonance multiplets are $\tau_0 \sim 450$, $N(\mathrm{Fe^+}) \sim 10^{15.5}\,(b/10)\,\mathrm{cm^{-2}}$ and $N(\mathrm{H}) > 10^{20.5}\,(b/10)\,\mathrm{cm^{-2}}$. Thus, if the self-absorption occurs in individual filaments, these have a lower limit to their columns about 100 times less than the column deduced from the X-ray continuum absorption. It follows that if the X-ray absorption arises in these filaments there are less than ~100 in our line of sight.

Returning to a general survey of weak features, those at λ2452 and λ2658 stand out most clearly in the longwave spectra. The former may be identified as O IV λλ2449.4, 2450.0 or with a strong unidentified line seen at λ2458.8 in RR Tel (Penston *et al.* 1981). The latter might plausibly be [Fe XI] λ2648.7, given the presence of [Fe XI] λ7892 in the infrared (Grandi 1978).

In the shortwave region the problems are worse because of the greater number of absorption lines. The discussion of Section 3 favoured continuum 'windows' at λλ1440–1470 and λλ1700–1710. Connecting these two points to the long wavelength spectrum near λ2000 and extrapolating if necessary provides the best continuum estimate, which in turn shows that several lines, e.g. C IV, O III] and possibly N III], have very broad wings. For the strongest lines, there is evidence that the extents of these wings are variable; this point is discussed further in Sections 5.2 and 6.

However, wings of strong lines cannot account for all the excess flux above the continuum. For example, the region between N V and O IV]/Si IV is consistently high, probably due to blending of emission from Si II λ1260, O I λ1302 and C II λ1335. A similar excess exists between N III] emission and the Al III absorption lines. This latter feature is also

present in active galaxies with strong optical Fe II spectra such as I Zw 1 and II Zw 136 (Snijders *et al.* 1980). It may be attributed to a blend of Fe II lines, notably in multiplets 191 and 65, which are moderately strong in the Sun, and the Si II lines λλ1808, 1816, 1817. Another possibility is to invoke a blend of Si II with strong unidentified lines found in the slow nova RR Tel (Penston *et al.* 1980) at λλ1776.6, 1832.0 and 1844.4.

The last feature deserving discussion in this section is the one on the red wing of the C IV line at a rest wavelength of λ1591 ± 2. This feature appears clearly on several of our spectra. Its wavelength is too long to be attributed to [Ne V] λ1575 (which might be weakly present) or Fe II multiplets 44 and 45, and too short to be [Ne IV] λ1602 or the CO fluorescence feature discussed by Bartoe *et al.* (1978). There are no lines seen near this wavelength in RR Tel (Penston *et al.* 1980); in the Sun Si I lines are identified (Burton & Ridgeley 1970) but do not seem a plausible explanation for NGC 4151. Davidsen & Hartig (1978) suggested an identification with O III but the absence of other stronger recombination lines argues against this possibility. Its identification thus remains a puzzle.

5.2 INTENSITIES

Emission line intensities are given in Table 6. They were computed by a purely impersonal method. First the adopted continuum points in the observed energy distribution (Section 3) were fitted by a two-component energy distribution

$$f_\nu = a\nu^0 + b\nu^{-2}. \quad (1)$$

The least-squares fits were generally good, with rms residuals less than $\sim 0.6 \times 10^{-14}$ erg $cm^{-2} s^{-1} Å^{-1}$. Then the total flux within a wavelength band including the line was summed from the data, and that corresponding to the continuum (1) in the same window was subtracted. This procedure was adopted because of the highly blended nature of the spectrum, in order to provide a clear and objective definition of line strength. However, not all the problems associated with blending can be removed, and the intensities listed in Table 6 (particularly in the shortwave region) must be judged with this in mind. For example, the intensities of the Si IV/O IV] blend and of C IV include a (negative) contribution from the variable absorption lines. Likewise the intensity of N IV] may include a positive contribution from the wing of C IV.

The accuracy of the intensities in Table 6 should be about ±10 per cent for strong lines and $\pm 0.1 \times 10^{-12}$ erg $cm^{-2} s^{-1}$ for weak lines; the latter derives from the observed scatter of continuum points about the fitted equation (1). The fit to the May data and its calibration are worse than normal, and larger errors of up to ±20 per cent or $\pm 0.3 \times 10^{-12}$ erg $cm^{-2} s^{-1}$ are expected.

The results presented in Table 6 suggest that all lines longward of and including the Si III]/C III] blend are constant to within the accuracies given above. By contrast, shortward of and including N III] the intensities all seem to vary from epoch to epoch. In the cases of C IV and the Si IV/O IV] blend the confusing effect of variable absorption has already been noted. Nevertheless, all the lines generally vary together. In particular, the intensity of the strong C IV feature varies in a similar way and by a similar relative amount to the sum of the intensities of weaker lines (the Si IV/O IV] blend, and the N IV], He II, O III] lines). This can hardly be due to any systematic error in the way the continuum is placed since such errors would preferentially affect weak lines.

It appears that the lines were strongest in 1978 May and October and weakest in 1979 January. A similar pattern is present for the Si III]/C III] blend but its amplitude is less than the ±10 per cent accuracy claimed. No such effect is seen in Mg II, C II]/[O III] or other

long wavelength lines. The reason may be that variations will not occur in the narrow forbidden lines, but only in lines of second or higher ions (e.g. in the H II region) excluding Mg II and C II] which may arise in a neutral transition region. Alternatively, variations may not be detected simply because the lines are too weak. Previous claims for variability of optical lines at Hα by Cherepashchuk & Lyutyi (1973) and in the He II Paschen series λ4686 and 3203 by Boksenberg *et al.* (1975) and Boksenberg & Penston (1976) are strongly supported by the present ultraviolet data. This variability is discussed again in Section 6.

It is, in principle, possible to use the line intensities of Table 6 to diagnose the physical state of the emitting gas. However, there are three reasons why caution argues against doing this here. First, some emission lines are variable and no corresponding optical data, for example, exist at our epochs. Secondly, the optical spectra indicate the presence of distinct broad and narrow line regions with very different physical properties, and these are not clearly distinguishable at *IUE*'s low resolution. Lastly, the general difficulty in disentangling blends, including with the absorption lines, also causes problems. It may be more appropriate to make plasma diagnoses when good high-dispersion data exist. However, it does seem worthwhile now to make just two remarks about the line intensities. Firstly, the C IV intensities of Table 6 confirm (Boksenberg *et al* 1978) that NGC 4151 clearly violates Baldwin's (1977) relationship between quasar C IV emission equivalent width and continuum luminosity at λ1450. Secondly, a meaningful intensity ratio can be given for the He II recombination lines λλ1640 and 4686, although this is necessarily rendered somewhat uncertain by possible absorption in λ1640 and by non-simultaneity of observation. After dereddening with $E(B-V) = 0.05$, the intensity ratio I_{1640}/I_{4686} lies in the range 5.7 to 1.2 depending on whether maximum or minimum values are chosen from Table 6 and Boksenberg *et al.* (1975). The recombination ratio is ~ 6.6 (Seaton 1978). This probable discrepancy is in the same sense as for the well-known Ly α/Hβ problem (see Davidsen 1980 for a review).

5.3 VARIABLE LINE WINGS

The presence of very wide line wings was noted in Section 5.1. In the case of C IV there is good evidence that these wings are variable with time. For example, compare the region between C IV and N IV] λ1486 at different epochs in Fig. 1. Similarly on the red side of C IV, the region between C IV and He II λ1640 is sometimes filled in and at other times seems to represent a continuum point. In 1978 May and October, the wings are fully 30 000 km s^{-1} wide at zero intensity whereas in 1979 January they are less than 20 000 km s^{-1}. There is evidence for a similar effect in Si IV. Note the great width of these lines compared to the 8000 km s^{-1} FWZI of the Balmer lines, although He I λ5876 seems intermediate at 12 000–16 000 km s^{-1} (Boksenberg *et al.* 1975; Osterbrock & Koski 1976).

Table 7. Value of the C IV linewidth index as a function of epoch.

Date	Linewidth index
1978 May	0.126
July	0.049
Aug	0.066
Oct	0.106
Dec	0.086
1979 Jan	0.043

Table 8. The C III] line through large and small apertures.

Date	Aperture	Peak intensity★ (10^{-14} erg cm^{-2} s^{-1} Å^{-1})	Total flux★† (10^{-12} erg cm^{-2} s^{-1})
1978 July 24	S	34	4.5
	L	40	5.3
1978 Oct 19	S	33	4.8
	L	44	6.6
1978 Dec 9	S	39	5.4
	L	39	5.8
1979 Jan 21	S	30	4.9
	L	33	5.2

★ After normalizing the flux scale using continuum regions; estimated relative uncertainty of the flux is $\pm 0.2 \times 10^{-12}$ erg cm^{-2} s^{-1}.
† Slight differences (within the quoted 10 per cent uncertainties) from the values of Table 6 are due to slightly different procedures used for this purpose.

To quantify this effect in a more satisfactory way, Table 7 presents values of a C IV 'line-width index' as a function of epoch. This index is defined as the fraction of flux in excess of the continuum (defined by equation 1) in the regions λλ1500–1519 and λλ1615–1634 compared to the total C IV intensity. This variability too is discussed further in Section 6.

In contrast to the C IV line, the wings on C III] λ1909 seem rather weak – weaker in fact than those on O III] in spite of the former's being a strong line overall. From this one can deduce that the density in the fastest moving parts of the broad line region lies between the critical densities of C III and O III, $10^{10} \lesssim n_e \lesssim 10^{11.5}$ cm^{-3} (Doschek *et al.* 1978).

5.4 EXTENDED C III] EMISSION

At four epochs, short wavelength spectra were taken through both large (20 × 10 arcsec) and small (3 arcsec diameter) apertures within one hour. After normalizing the spectra one to the other, one can check that the broad lines and continuum have the same ratio between large and small apertures as they would if they were point sources. However, it is found that the C III]/Si III] blend is consistently and significantly weaker in the small aperture (see Table 8) in both integrated flux and peak intensity. This is in spite of the fact that any resolution difference would enhance the peak flux of the narrow C III] line.

This is another indication (see also Penston *et al.* 1979) that the C III] line has a major component from the extended 'narrow-line' region. The narrow-line region is known from optical data to extend to at least 6 arcsec in diameter (Ulrich 1973) – or 150 pc at NGC 4151 if $H_0 = 50$ km s^{-1} Mpc^{-1}.

6 Variations

6.1 GENERAL

NGC 4151 is known to be variable in the infrared (Lebofsky & Rieke 1980), in the optical continuum (e.g. Penston *et al.* 1974) and lines (Anderson 1974; Cherespashchuk & Lyutyi 1973) and in X-rays (Barr *et al.* 1977). Previous ultraviolet work (Boksenberg *et al.* 1978) has found it variable here too.

The present study was unfortunately not closely associated with work at other wavelengths but in the earlier sections are reported many distinct parameters that vary with time, based on *IUE* data alone:

(i) FES magnitudes;
(ii) long wavelength continuum;
(iii) short wavelength continuum;
(iv) strengths of high-excitation absorption lines (N V, C IV and Si IV);
(v) strengths of lower-excitation absorption lines (Al III and Si II);
(vi) V/R ratio of the composite C IV feature;
(vii) short wavelength region emission line strengths; and
(viii) the C IV linewidth index.

It is now necessary to reduce the confusion inherent in these eight different types of variations, and to this end the relationships between them are discussed in the next sections.

6.2 THE CONTINUUM VARIABILITY

Fig. 6 presents the light curves in the blue (from the FES) and for the long and short wavelength parts of the ultraviolet spectra. The long wavelength intensity is represented by the flux at λ2500 (log ν = 15.08) computed from the fit to the long wavelength data points of Table 3. The short wavelength intensity is represented by the flux at λ1455 (log ν = 15.31). The 1978 May points are bracketed as uncertain since their normalization follows from fixing the C III] emission intensity by reference to other epochs, no large-aperture data being available for May.

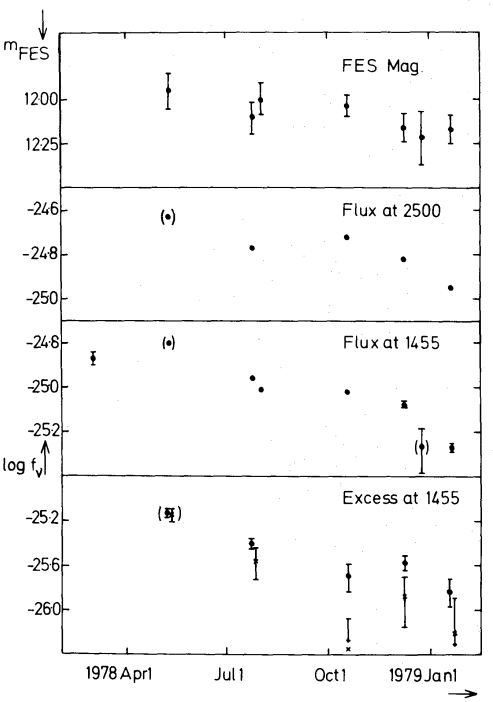

Figure 6. Continuum flux variations with time. Error bars are plotted unless they would be smaller than the plotted symbols. At the top, the FES magnitudes (~ 4700 Å) are plotted at double the vertical scale of the other parts to compensate for contamination by starlight. Bracketed points are (1978 May) calibrated by assuming Mg II and C III] line intensities are constant and (1978 December 25) measured from a high dispersion spectrum (Penston *et al.* 1979). At the bottom the excess fluxes at 1455 Å over a power law extrapolation of the long wavelength points fitted before (closed circles) and after (crosses) dereddening by 0.05 mag. Such pairs of points may be plotted separated in time for clarity.

The differences between the behaviour of these short- and long-wavelength representative intensities reflect the results of Table 3 concerning the possible existence of distinct long and short wavelength components. They are, after all, derived from the same data. The flux at λ2500 is high in 1978 May and October and low in 1979 January. At λ1455 the same curve is skewed downward at later times so that there is a somewhat greater range of variation. In Table 3 this corresponds to a decline of the short wavelength excess. This may indicate a different temporal behaviour of long and short wavelength components. However, this difference is not yet completely convincing, given the similarity of the long and short wavelength light curves in Fig. 6. It will be tested further using more data (Paper II).

The FES light curve is consistent with the long wavelength behaviour. Note that the FES light curve is plotted in Fig. 6 at effectively twice the vertical scale to compensate for the dilution of the nuclear source by starlight.

The time-scale of the variations may be shorter than the spacing between the observations, which is of the order of one month. Variations on this time-scale and with comparable amplitude have been found in the optical and near infrared (Penston *et al.* 1974; Lebofsky & Rieke 1980).

Strong variability is present also in the 1–20 keV region of the spectrum. Here the situation is rather complex (see Lawrence 1980, and references therein). Flaring activity, with increases of up to about five times the average intensity, is observed to occur on a time-scale of days, and on one occasion at least (Tananbaum *et al.* 1978) a flare was detected with a duration of approximately 12 min. Moreover, changes have been observed in the soft X-ray cut-off with a range in the column density N_H of the absorbing gas of $(3.5–18) \times 10^{22}$ cm^{-2}. No variability has been reported so far in the range 20–100 keV. Above 100 keV the most recent measurements quoted in Section 3.3 indicate that the source may be strongly variable.

It would be extremely interesting to investigate whether ultraviolet variability also occurs on time-scales as fast as those observed in the medium energy X-rays. The present data give no evidence of variations between spectra taken a few hours apart, but clearly one would need to monitor the object day by day over a long period of time. Boksenberg *et al.* (1978) found a possible three-fold increase in the short wavelength range comparing their spectrum taken 1978 February 11 with the previous day's rocket measurement by Davidsen & Hartig (1978). A marginally significant increase between these days was detected by *Ariel V* (Lawrence 1980).

6.3 ABSORPTION LINE VARIABILITY

Changes in strengths of absorption lines are presented in Figs 7 and 8 and may be compared with the continuum variations of Fig. 6. The data reveal a direct correlation between the intensity of the continuum flux and the strength of lines of the highly ionized species Si IV, C IV and N V. The flux increase between 1978 July and October, followed by the decrease to the minimum value in 1979 January, is mirrored by a similar pattern of variation of the high ions. In addition, the continuum maximum of 1978 May is coincident with a great strengthening of N V. In contrast, lines of lower ions show generally smaller variations which are not easily identifiable with changes in the continuum strength, except for Al III λ1857 and Si II + Si II* λ1260–1265, which may be anticorrelated with the high ionization lines.

Anderson (1974) found the strengths of the Balmer and He I λ3889 absorption lines to be anticorrelated with changes in the optical continuum. He concluded that the relative populations of metastable levels of H I and He I are governed, through photo-ionization, by the brightness of the central source. The present results provide additional evidence to support this conclusion. If the relative populations of two successive ionization stages, $n(X^i)$ and $n(X^{i+1})$, are determined by a balance between photo-ionization and recombi-

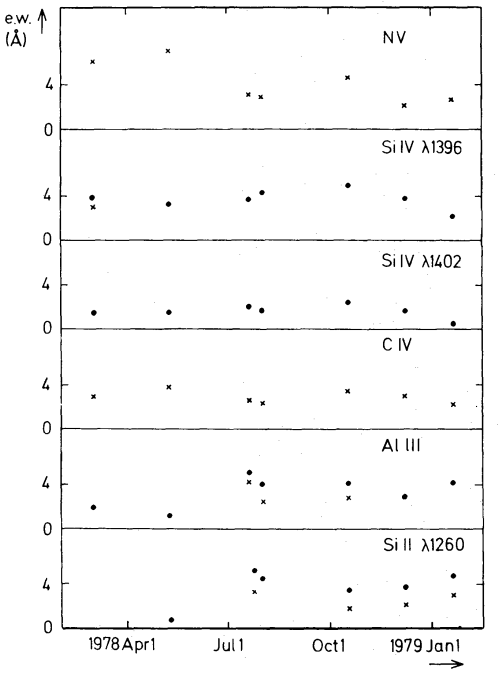

Figure 7. Behaviour of absorption line equivalent widths as a function of time for lines believed variable. Closed circles represent the values corresponding to a 'high' local continuum, crosses to a 'low' continuum (for more discussion, see text). Note the correlation of N V, Si IV and C IV and anticorrelation of Al III and Si II λ1260 with the 2500 Å continuum (Fig. 6).

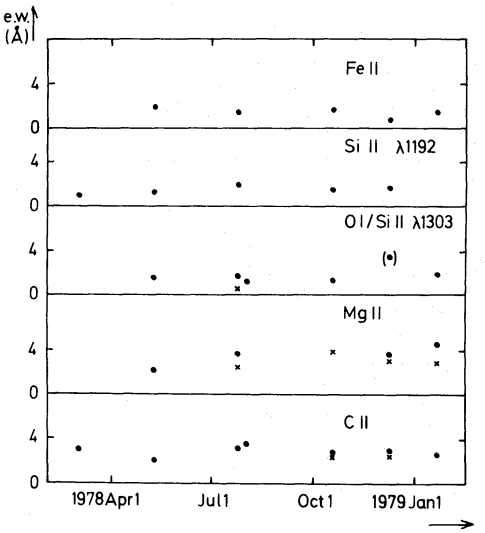

Figure 8. Behaviour of absorption line equivalent widths as a function of time for presumed non-variable first ions. Symbols as in Fig. 7.

nation processes, qualitatively one may expect that variations in the ionizing flux will be reflected most sensitively by certain species of ions.

The details of ionization balance will determine whether the derivative of $n(X^i)$ with respect to the photo-ionization rate is positive, negative or zero. Such effects may explain the observed strengthening of the high ions and the weakening of Al III and Si II* as the ultraviolet source brightens, and the fact that N V responded most sensitively to the high continuum flux.

Anderson (1974) pointed out that the anticorrelation between the Balmer absorption lines and continuum on a time-scale of 15 day implies $n_e > 5 \times 10^6 \text{ cm}^{-3}$. This is consistent with the absorptions occurring in or near the broad emission line region. Limits to the density are also obtained by applying similar arguments to the present results, but the limits are less stringent since the time intervals over which there is a significant correspondence between continuum flux and absorption line strengths are longer. More closely spaced observations of the variable ultraviolet absorption lines are required in order to improve current estimates of the gas density and distance from the central source. This is because the recombination rates of the ions in question are greater than those of H I and He I (Aldrovandi & Pequignot 1973).

6.4 EMISSION LINE VARIABILITY

Fig. 9 shows the changes of intensity against epoch for Lyman α, C IV and the sum of the other lines shortward of λ1800 in Table 6. As noted in Section 5.2, the changes in each are similar one to another and also resemble the variations of the continuum. While some part of the variation in the weak lines might be attributed to systematic errors in continuum fitting, this can hardly be true for the strong Lyman α and C IV lines. We conclude that the variation of some emission lines is a real effect.

The explanation advanced in the last section for the absorption line variation in terms of photo-ionization by a variable continuum may apply here too. Recent work on the formation of Mg II and Fe II emission lines in active nuclei suggests they may be formed in an extended H I region (Collin-Souffrin *et al.* 1980; Netzer 1980). Their lack of variation could indicate that these lines arise in a different and more extended region than that of the high ionization lines, confirming this theoretical picture.

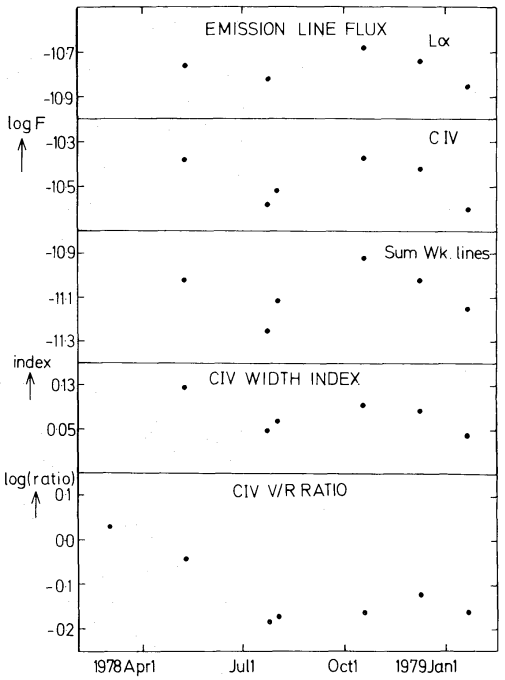

Figure 9. Variation of emission line intensities with time. The sum of weak lines refers to the lines in Table 6 shortward of 1800 Å other than Lα and C IV to which it is compared. The linewidth index is the ratio of flux in the wings of the C IV line to the total intensity. Note the correlations of the above quantities with the 2500 Å continuum (Fig. 6). At the bottom the variation of the violet-to-red emission peaks in the C IV profile is shown.

The C IV linewidth index is also presented in Fig. 9 as a function of epoch, and again the same form of variation is apparent. High velocities are absent when the continuum is faint. Although other interpretations cannot be excluded, most plausibly the highest velocities occur nearest to the nucleus. This is true of general models of accretion on to massive condensed objects, where the broad-line emitting material may be considered a tracer of the accreting fluid (e.g. Maraschi *et al.* 1980). It is tempting then to interpret the positive correlations between the strength of the continuum, the linewidth index, and intensity of C IV, as evidence in favour of such models where the nuclear power is effectively regulated by the rate at which the accretion fuel is supplied.

To pursue speculations of this or other sorts, one would like to have some information on the density of the material producing the extended wings (actually the bulk of the C IV line) which may be wider than any other lines in this object. As noted in Section 5.3, the C III] λ1909 line is most convincingly narrower since this line is relatively strong overall. Whether some other lines (e.g. O III]) seem narrower simply because they are weaker is hard to say given the many blends in the spectrum. However, the range of densities $10^{10} \lesssim n_e \lesssim 10^{11.5}$ cm^{-3} derived in Section 5.3 applies to that part of the accretion flow with velocities between about 4000 and 10 000 km s^{-1}.

It seems, therefore, that most of the variable parameters listed in Section 6.1 are correlated or anticorrelated with the continuum flux. As discussed above it is uncertain whether the behaviours of the long- and shortwave components are truly different, but if they are, then the variations are with the long wavelength component. Since this would be surprising, it may be worthwhile to speculate on this point. The photo-ionization arguments associate changes in the highly ionized species with continuum changes, mainly at energies of 33–77 eV (i.e. λ375 to 160 Å). This would suggest either a geometry in which the emission/absorption line region is far from (or shielded from) the source of the *IUE* short wavelength component, or that the short wavelength' source in fact contributes little flux below ~ λ500 Å and the 'long wavelength' component again dominates. In the latter case, the short wavelength component then might plausibly be a blackbody (or a combination of blackbodies) with temperature near 30 000 K. In any case, the short wavelength component must turn down rather quickly to avoid conflict with the X-ray data, which would suggest a similar conclusion but allow a higher temperature for the blackbody. The source of such a component is uncertain but might be an assemblage of super-dense filaments in which the line emission is suppressed (Ulrich *et al.* 1980) or else an optically thick disc.

6.5 *V/R* RATIO VARIATIONS

The other two variable parameters are presented in Figs 6 and 9. In Fig. 9 is the log of the *V/R* ratio of Table 7; in Fig 6 the short wavelength excess of Table 3 is presented. There is some resemblance in the form of their variations, although the amount of data is very small, but both seem different from the more or less common behaviour of the other parameters.

In connection with the C IV *V/R* ratio, it is interesting to recall that the central absorption in C IV was absent in the data of Davidsen & Hartig (1978) taken on 1978 February 10. Any absorption as strong as that seen in all *IUE* data at all epochs should have been visible even at Davidsen & Hartig's factor-of-2 poorer resolution. It is tempting therefore to associate the appearance of C IV absorption with the rapid brightening seen between 1978 February 10 and the *IUE* observations one day and two weeks later. Thereafter the absorption certainly gradually shifted to positive velocities, stabilizing in early 1978 August. Continuing monitoring of NGC 4151 in the ultraviolet is necessary in order to look for any repetition of such an event.

7 Future work

This is not the last paper on the ultraviolet spectrum of NGC 4151. However, we believe that this paper at least starts the process of bringing some order to the variety of variable phenomena present which initially was so confusing.

Of course, *IUE* high dispersion data may add considerably to our knowledge of NGC 4151. Detailed profiles of emission and absorption lines can be obtained in this way. Some work has been published (Penston *et al.* 1979) but it needs extending to the long wavelength range and, given the variability of NGC 4151, to several epochs. When such improved emission line profile data is available, it will become possible to assess line ratios relevant to the various regions for diagnosis of physical conditions. Variations in absorption line velocities will also be more easily studied. However, because of the necessarily weak signals at high dispersion, development of refined image processing methods is mandatory to enable progress to be made in this area.

The present results show that several absorption lines arise from metastable levels. Further considerations of the relative populations of ground, fine-structure and metastable levels could yield important information on the degree of excitation of the gas and on its distance from the central source. This, together with a more detailed analysis of ionization-balance conditions determining the variable strengths of absorption and emission lines, will allow a fuller picture to be constructed of the geometry and physical properties of material in the nuclear regions of NGC 4151.

Another important need for future study is to probe the variability of NGC 4151 on shorter time-scales, and to arrange simultaneous monitoring in other wavebands.

We shall return to these and other topics in later papers.

Acknowledgments

We thank the ESA and SRC selection committees for generously supporting these observations. GCP and EGT thank B. Falconi and G. Sechi and acknowledge financial support from CNR.

References

Aldrovandi, S. M. V. & Pequignot, D., 1973. *Astr. Astrophys.*, **25,** 137.
Anderson, K. S., 1974. *Astrophys. J.*, **189,** 191.
Anderson, K. S. & Kraft, R. P., 1969. *Astrophys. J.*, **158,** 859.
Baity, W. A. *et al.*, 1975. *Astrophys. J.*, **199,** L5.
Baldwin, J. A., 1977. *Astrophys. J.*, **214,** 679.
Baldwin, J. A. & Netzer, H., 1978. *Astrophys. J.*, **226,** 1.
Baldwin, J. *et al.*, 1979. *The First Year of IUE*, p. 126, ed. A. J. Willis, University College London.
Barr, P., Ives, J. C., Sanford, P. W. & White, N. E., 1977. *Mon. Not. R. astr. Soc.*, **181,** 465.
Bartoe, J.-D. F., Brueckner, G. D., Sandlin, G. D., Van Hoosier, M. E. & Jordan, C., 1978. *Astrophys. J.*, **223,** L51.
Boggess, A. *et al.*, 1978a. *Nature (Lond.)*, **275,** 372.
Boggess, A. *et al.*, 1978b. *Nature (Lond.)*, **275,** 377.
Bohlin, R. C., Savage, B. D. & Drake, J. F., 1978. *Astrophys. J.*, **224,** 132.
Bohlin, R. C., Holm, A., Savage, B. D., Snijders, M. A. J. & Sparks, W. M., 1980. *Astr. Astrophys.*, **85,** 1.
Boksenberg, A., Shortridge, K., Allen, D. A., Fosbury, R. A. E., Penston, M. V. & Savage, A., 1975. *Mon. Not. R. astr. Soc.*, **173,** 381.
Boksenberg, A. & Penston, M. V., 1976. *Mon. Not. R. astr. Soc.*, **177,** 127P.
Boksenberg, A. *et al.*, 1978. *Nature (Lond.)*, **275,** 404.
Boksenberg, A. *et al.*, 1980. *Second European IUE Conference (ESA SP-157)*, p. lxvii, eds Fitton, B. & Grewing, M., European Space Agency, Paris.

Burton, W. M. & Ridgeley, A., 1970. *Solar Phys.*, **14**, 3.
Cassatella, A. & Ponz, D., 1979. *ESA IUE Newsletter, No. 4*, p. 5.
Cherepashchuk, A. M. & Lyutyi, V. M., 1973. *Astrophys. Lett.*, **13**, 165.
Collin-Souffrin, S., Dumont, S., Heidman, N. & Joly, M., 1980. *Astr. Astrophys.*, **83**, 190.
Cromwell, R. H. & Weymann, R., 1970. *Astrophys. J.*, **159**, L147.
Davidsen, A. F. & Hartig, G. F., 1978. *Paper read at COSPAR/IAU Symposium on X-ray Astronomy*, Innsbruck, June.
Davidsen, A. F., 1980. *IAU Symp. 92: Objects of High Redshift*, p. 235, eds Abell G. O. & Peebles, P. J. E., Reidel.
de Boer, K. S. & Savage, B. D., 1980. *Astrophys. J.*, **238**, 86.
de Bruyn, A. G. & Sargent, W. L. W., 1978. *Astr. J.*, **83**, 1257.
de Bruyn, A. G. & Willis, B. J., 1974. *Astr. Astrophys.*, **33**, 351.
Doschek, G. A., Feldman, U., Bhatia, A. K. & Mason, H. E., 1978. *Astrophys. J.*, **226**, 1129.
Elias, J. H. *et al.*, 1978. *Astrophys. J.*, **220**, 25.
Fogarty, W. G. *et al.*, 1971. *Astr. J.*, **76**, 537.
Gillett, F. C., Forrest, W. J., Merrill, K. M., Capps, R. W. & Soifer, B. T., 1975. *Astrophys. J.*, **200**, 609.
Grandi, S. A., 1978. *Astrophys. J.*, **221**, 501.
Gursky, H., Kellogg, E. M., Leong, C., Tananbaum, H. & Giacconi, R., 1971. *Astrophys. J.*, **165**, L43.
Holt, S. A., Mushotsky, R. F., Becker, R. H., Boldt, E. A., Serlemitsos, P. J., Szymkowiak, A. E. & White, N. E., 1980. *Astrophys. J.*, **241**, L13.
Ives, J. C., Sanford, P. W. & Penston, M. V., 1976. *Astrophys. J.*, **207**, L159.
Jordan, C., 1979. *Progress in Atomic Spectroscopy, Part B*, p. 1453, eds. Hanle W. & Kleinpoppen, H. Plenum, New York.
Kellerman, K. I. & Pauliny-Toth, I., 1968. *Astr. J.*, **73**. 874.
Lawrence, A., 1980. *Mon. Not. R. astr. Soc.*, **192**, 83.
Lebofsky, M. J. & Rieke, G. H., 1980. *Nature (Lond.)*, **284**, 410.
Maraschi, L., Perola, C. G. & Treves, A., 1980. *Astrophys. J.*, **241**, 910.
Meegan, C. A. & Haymes, R. C., 1979. *Astrophys. J.*, **233**, 510.
Morton, D. C., 1978. *Astrophys. J.*, **222**, 863.
Morton, D. C. & Smith, W. H. 1973. *Astrophys. J. Suppl.*, **26**, 333.
Mushotsky, R. F., Holt, S. S. & Serlemitsos, P. J., 1978. *Astrophys. J.*, **225**, L115.
Mushotsky, R. F., Marshall, F. E., Boldt, E. A., Holt, S. S. & Serlemitsos, P. J., 1980. *Astrophys. J.*, **235**, 377.
Nachman, P. & Hobbs, L. M., 1973. *Astrophys. J.*, **182**, 481.
Netzer, H., 1980. *Astrophys. J.*, **236**, 406.
Noerdlinger, P. D. & Dynan, S. E., 1975. *Astrophys. J. Suppl.*, **29**, 185.
Nussbaumer, H., 1977. *Astr. Astrophys.*, **58**, 291.
Nussbaumer, H. & Schild, H., 1979. *Astr. Astrophys.*, **75**, L17.
Osterbrock, D. E., 1962. *Astrophys. J.*, **135**, 195.
Osterbrock, D. E., 1977. *Astrophys. J.*, **215**, 733.
Osterbrock, D. E. & Koski, A. T. 1976. *Mon. Not. R. astr. Soc.*, **176**, 61P.
Penston, M. V., Penston, M. J., Selmes, R. A., Becklin, E. E. & Neugebauer, G., 1974. *Mon. Not. R. astr. Soc.*, **169**, 357.
Penston, M. V., Clavel, J., Snijders, M. A. J., Boksenberg, A. & Fosbury, R. A. E., 1979. *Mon. Not. R. astr. Soc.*, **189**, 45P.
Penston, M. V., Benvenuti, P., Cassatella, A., Heck, A., Selvelli, P., Macchetto, F., Ponz, D., Jordan, C., Cramer, N., Rufener, F. & Manfroid, J., 1981. *Mon. Not. R. astr. Soc.*, in preparation.
Perotti, F., Della Ventura, A., Sechi, G., Villa, G., Di Cocco, G., Baker, R. E., Butler, R. C., Dean, A. J., Martin, S. J. & Ramsden, D., 1979. *Nature (Lond)*. **282**, 484.
Rieke, G. H., 1978. *Astrophys. J.*, **226**, 550.
Savage, B. D. & de Boer, K. S., 1981. *Astrophys. J.*, **243**, 460.
Schmidt, G. D. & Miller, J. S., 1980. *Astrophys. J.*, **240**, 759.
Seaton, M. J., 1978. *Mon. Not. R. astr. Soc.*, **185**, 5P.
Seaton, M. J., 1979. *Mon. Not. R. astr. Soc.*, **187**, 75P.
Snijders, M. A. J., 1979. *SRC IUE Newsletter, No. 4*, p. 15.
Snijders, M. A. J., 1980. *SRC IUE Newsletter, No. 5*, p. 85.
Snijders, M. A. J., Boksenberg, A., Haskell, J., Fosbury, R. A. E. & Penston, M. V., 1980. *Second European IUE Conference (ESA SP-157)*, p. 279, eds. Fitton, B. & Grewing, M., European Space Agency, Paris.
Sramek, R. A., 1975. *Astr. J.*, **80**, 771.

Stickland, D., 1980. *ESA IUE Newsletter, No. 5,* p. 30.
Tananbaum, H., Peters, G., Forman, W., Giacconi, R., Jones, C. & Arni, Y., 1978. *Astrophys. J.,* **223,** 74.
Thomson, I., Landstreet, J. D., Angel, J. R. P., Stockman, H. S., Woolf, N. J., Martin, P. G., Maza, J. & Beaver, E. A., 1979. *Astrophys. J.,* **229,** 909.
van der Kruit, P., 1971. *Astr. Astrophys.,* **15,** 110.
Ulrich, M. H., 1973. *Astrophys. J.,* **181,** 51.
Ulrich, M. H. *et al.,* 1980. *Mon. Not. R. astr. Soc.,* **192,** 561.
Wampler, E. J., 1971. *Astrophys. J.,* **164,** 1.
White, R. S., Dayton, B., Gibbons, R., Long, J. L., Zanrosso, E. M. & Zych, A. D., 1980. *Nature (Lond).,* **284,** 60.
Wills, B. J., Netzer, H., Uomoto, A. K. & Wills, D., 1980. *Astrophys. J.,* **237,** 319.
Wu, C. C. & Weedman, D. W., 1978. *Astrophys. J.,* **223,** 798.